MEDDOCS Open Access Publisher

ISSN: 2578-8760

Journal of Nanomedicine

Open Access | Research Article

Advancement in Wound Healing by the Application of Folate Functionalized Metallic Colloidal Antibiotherapy

Roxane Abdel-Gawad*; Rihab Osman; Gehanne AS Awad; Nahed Mortada

Department of Pharmaceutics and Industrial Pharmacy, Faculty of Pharmacy, Ain Shams University, P.O. Box 11566, Cairo, Egypt.

***Corresponding Author(s): Roxane Abdel Gawad**

Department of Pharmaceutics and Industrial Pharmacy, Faculty of Pharmacy, Ain Shams University, P.O. Box 11566, Cairo, Egypt.

Email: roxanne_abdelgawad@pharma.asu.edu.eg

Received: Dec 01, 2024

Accepted: Jan 06, 2025

Published Online: Jan 13, 2025

Journal: Journal of Nanomedicine

Publisher: MedDocs Publishers LLC

Online edition: http://meddocsonline.org/

Keywords: Silver nanoparticles; Folic acid; Cefotaxime sodium; Green synthesis; Antibacterial activity; Wound healing.

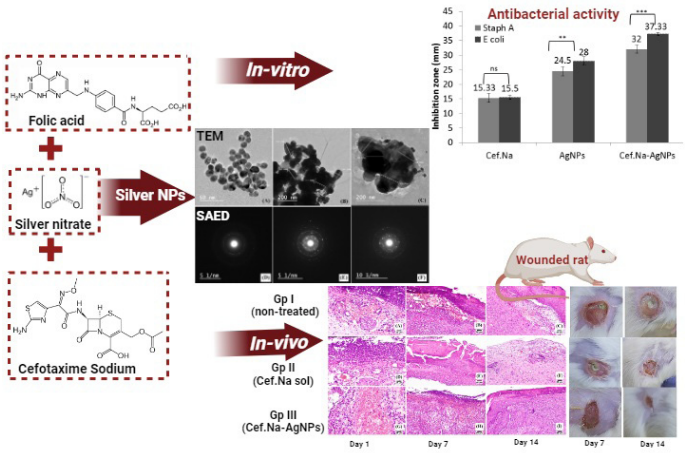

Graphical abstract

Abstract

Folic Acid (FA) is introducing itself as a useful addition to wound management protocol. Herein, we report a novel eco-friendly method to prepare silver nanoparticles (Ag-NPs) using the anabolic FA as a reducing agent. The synthesis of FA-stabilized AgNPs (FA-AgNPs) was confirmed by spectrophotometric analysis, revealing the presence of the characteristic absorption peak corresponding to the *Surface Plasmon Resonance* of colloidal FA-AgNPs. FA intercalation in the colloidal AgNPs was proved by EDX, FTIR and UV spectrophotometry. FA-AgNPs loaded with cefotaxime sodium (cef.Na) demonstrated a synergistic antibacterial activity against both gram-positive and gram-negative. Superior cell survival, using normal skin fibroblasts, was proved in the presence of FA, in addition to enhanced cell survival at high Ag content due to the large-sized particles obtained. The wound healing activity, evaluated in injured rats, showed more than 85% of wound closure after 2 weeks. As healing proceeds, the oxidative stress decreases as delineated by a decrease in Malondialdehyde (MDA) and an increase in Superoxide Dismutase (SOD) levels.

Statement of significance: This study focuses of synthesizing silver nanoparticles in an eco-friendly way using anabolic folic acid, then loading it with a broad spectrum antibiotic, cefotaxime sodium. This environmentally safe green method produced colloidal nanoparticles combining the synergistic antibacterial potential of silver and the antibiotic, producing low mutagenic risk potion, considered an illuminated hope to control and prevent microbial resistance. Folic acid being engulfed in the silver nanoparticles decorated with cefotaxime sodium produced a mosaic working in harmony to achieve clean rapid and scar-less wound healing in short time frame. Such combination could be easily loaded on biogenic wound dressings' platform to facilitate its application on wounded surface.

Cite this article: Abdel-Gawad R, Osman R, Awad GAS, Mortada N. Advancement in Wound Healing by the Application of Folate Functionalized Metallic Colloidal Antibiotherapy. J Nanomed. 2025; 8(1): 1070.

Introduction

The complexity of the physiological process involved in wound healing substantiates the selection of suitable bioactive compounds that facilitate the various phases involved: cell growth, re-epithelialization, deposition of collagen fibers, and tissue regeneration. Recent studies have reported that the pavement of the path for promoting a rapid and complete wound healing is through a combinatorial application of several material such as Ag, biological material and drugs [1].

Topical application of folate derivatives has proved a marked decrease in inflammation with an enhanced tissue repair [1]. Furthermore, *Duman et al* proved an increased immune cell migration to the injured areas, potentiating collagen secretion through fibroblast stimulation, thus helping in improved wound healing [2]. The potential efficacy of FA was attributed to its ability to induce a strong anabolic state in the body by acting as a coenzyme in DNA and RNA synthesis, stimulating the gluconeogenesis, and the biosynthesis of collagen in the wound tissues [3,4]. FA, also called folacin (vit B9), is involved in cell multiplication, regulation of genetic activity, blood cells production, skin renewal, besides its strong reported antioxidant activity [5].

Metal-based nanoparticles as AgNPs are the most popular inorganic NPs regarded as a good contestant in tackling the demanding challenge of bacterial resistance to antibiotics. These powerful nano-weapons use mechanisms of action completely different from traditional antibiotics, making them able to eradicate many resistant bacterial strains. They have the ability to damage the bacterial cell membrane through formation of several depths and gaps, leading to leakage of cytoplasmic contents and cell death [6,7]. When AgNPs penetrate inside the microbial cell, the released Ag interacts with cellular structures and biomolecules such as proteins, enzymes, lipids, and DNA due to their affinity to P and S, making them nonfunctional [6]. Furthermore, AgNPs produce high levels of Reactive Oxygen Species (ROS) and free radical species such as hydrogen peroxide, superoxide anion, hydroxyl radical, hypochlorous acid and singlet oxygen, leading to death by posing an oxidative stress [7].

Besides the importance of green synthesis in generating a yield of AgNPs free from dangerous and undesirable secondary unwanted products; it allows for the incorporation of important entities within the structure of NPs especially during ripening stage. The presence of these biomaterials impart or potentiate special actions for the NPs as anticancer, antimicrobial, or antioxidant activities according to the reducing molecule potentials [8-12]. Herein, we focused on enhanced tissue regeneration by the natural, anabolic FA used to prepare AgNPs.

However, resistance to AgNPs was recently encountered by some mobile bacteria by coding periplasmic Ag-binding chaperone proteins that can efflux Ag ions out of the microorganism [13]. The combination of AgNPs with conventional antibiotics is a smart low mutagenic risk combination with synergistic activity to eradicate resistant strains at lower doses [10,11]. In this work, the optimized biogenic FA stabilized AgNPs were loaded with a broad spectrum antibiotic from the cephalosporins group, cefotaxime sodium (cef.Na). It has a significant antibacterial potential against most strains of bacterial pathogens responsible for various types of infections [16].

Experimental

Materials and methods

Cefotaxime sodium: Given as gift from ZHUHAI united company, Zhuhai, China. Folic acid: DSM-Switzerland. Silver nitrate ($AgNO_3$): Fisher Scientific, UK. Sodium bicarbonate ($NaHCO_3$) and formaldehyde solution: El gomhouria Pharmaceutical Chemicals, Cairo, Egypt. Ultra-pure water: MilliQ Plus, Millipore Iberica, Spain. Dialysis tubing cellulose membrane, Hematoxylin & Eosin stain (H&E): Sigma-Aldrich, UK. Molecular weight cut-off: 14,000 Daltons. Muller Hinton agar, Soyabean Casein Digest Medium (Tryptone Soya Broth) and Luria Bertani broth (LB): (HiMedia laboratories). Barium chloride: National Company. Sulphuric acid: Piochem laboratory. Living microorganisms (*Staphylococcus Aureus* and *Esherishia Coli*) and Animals: Male Albino rats (200 g, 6–8 weeks old). Fibroblast normal cell line HFB4, Dulbecco's Modified Eagle's Medium (DMEM), fetal bovine serum: from the *cell culture unit* in *center for drug discovery research and development* at faculty of pharmacy Ain Shams University.

Synthesis of FA-AgNPs

Three mL FA solution containing sodium bicarbonate ($NaHCO_3$) were dropped in 30 mL $AgNO_3$ solution, 1mM, brought to boil on a heated magnetic stirrer (*Yellow line, MGA HS 7, IKA, Germany*). The mixture was stirred for 5min, followed by a 60 min agitation at room temperature. Six $AgNO_3$/FA molar ratios were investigated, while $NaHCO_3$ concentration was raised from 1:1 to 1:8 weight ratio of FA to $NaHCO_3$ at each tested $AgNO_3$/FA ratio, leading to a set of 24 formulae (Table 1).

The plain formula was then dialyzed against 500 mL deionized water for 24h using a semipermeable membrane (molecular weight cut-off of 14,000 Daltons) to remove excess FA. The dialysate was analyzed spectrophotometrically till absence of FA. Thereafter, cef.Na was loaded at cef.Na/$AgNO_3$ 1:5 and 1:10 molar ratios by allowing specific volumes of drug solution to drop in the dialyzed FA-AgNPs dispersion and stirring was continued overnight at room temperature. The colloidal dispersions were then stored at 4°C for four weeks for stability monitoring.

AgNPs were also prepared using trisodium citrate (TSC) as a standard conventional reducing agent for comparison. $AgNO_3$ (at 1mM) was reduced using TSC at molar ratio $AgNO_3$ to TSC of 1:5, using 40% glycerol as stabilizer.

Characterization of FA-AgNPs

Particle size (PS) and zeta potential (ζ)

The PS was measured using dynamic light scattering particle size analyzer (Zetasizer) **(***Malvern nano ZS, Malvern instruments, UK*), after sample dilution to achieve a count rate of 200-300 kilo counts/second (Kcps) [17]. The surface charge, expressed as ζ, was also determined by the eletrophoretic mobility in a capillary cell with a 4mW He-Ne laser at a wavelength of 633nm at 25˚C [18].

Spectrophotometric analysis

Determination of λ_{max} of FA-AgNPs

The maximum absorbance was recorded using a UV spectrophotometer **(***Shimadzu, model UV-1601 PC, Koyoto, Japan*). The λ_{max} was noted as indicative for effective reduction of silver ions to AgNPs [19].

Ultraviolet (UV) spectrophotometric assay of cef.Na

The UV spectrum of cef.Na was first determined and the λ_{max} was recorded. The calibration curve of cef.Na was constructed

in phosphate buffer saline (PBS) solution, pH 7. The absorbances of serial dilutions of cef.Na, 10-70µg/mL, were recorded at FA λ_{max} using the 1st derivative technique.

In-vitro cef.Na release from FA-AgNPs

The *in-vitro* release was performed using the dialysis technique. An accurate volume of 500µL of cef.Na loaded FA-AgNPs was dialyzed against 5mL PBS using a semipermeable membrane. The sink conditions were fulfilled by the use of a total cef. Na of 3µg/mL [16]. The entire set was put in a thermostatically controlled shaking water bath (*Kotterman, Hanigsen, Germany*) operated at 100 strokes/min and at temperature of 37±0.5°C [20]. Accurately, 500µL samples were withdrawn at different time intervals (5, 10, 15, 30, 60, and 120 min) and substituted with the same volume of fresh medium to keep the external volume constant at 5mL. The cumulative percent of cef.Na released at each time interval was determined spectrophotometrically using the 1st derivative technique. The results obtained were compared to those of the same amount of the drug dissolved in DW operated at the same condition as the drug loaded formula.

Transmission electron microscope (TEM)

Transmission electron microscope **(***JEOL, HR-TEM, model: JEM-2199, Japan*) was used to visualize the selected NPs. A volume of 50µL sample of the freshly prepared optimized formula was taken and placed carbon-coated grid and left to dry. The sample was viewed under the microscope at 100 k fold enlargements at an accelerating voltage of 100 kV [21].

Selected area electron diffraction (SAED) was also measured using the same device. In this technique, parallel beams of high energy electrons pass through thin sample sections; their trajectories are altered by interactions with the atomic structure of the sample. The resultant diffraction pattern is then analyzed to determine the crystal structure of the sample material [22].

X-ray powder diffraction (XRPD)

XRPD was performed on pure $AgNO_3$, FA, cef.Na and the selected freeze dried formulae using an X-ray diffractometer (*Philips, PW 3710, USA*). The diffractogram of each sample was recorded with a scan speed of 4°min^{-1} in the range of 5–80° and at 40 KV and 30 mA [23].

Energy dispersive X-ray spectroscopy (EDX)

Lyophilized selected sample was placed onto a carbon coated copper grid and was used for analysis. A high resolution Scanning Electron Microscope (SEM) with energy dispersive X ray analyzer (EDX) **(***Stereoscam 90B, Cambridge Instruments-Cambridge, UK*) was operated at 20 kV [24].

Fourier transform infrared spectroscopy (FT-IR)

FT-IR spectra of the plain FA-AgNPs, cef.Na-FA-AgNPs and their individual components were recorded using potassium bromide (KBr) disc method using Fourier transform infra-red spectrophotometer (*Perkin-Elmer, USA*). Each sample was gently triturated with powdered KBr in a weight ratio of 1:100 and then pressed using a hydrostatic press at a pressure of 10 tons for 5 min. The disc was placed in the sample holder and was scanned from 4000 to 400cm^{-1}. All spectra were recorded at ambient temperature under vacuum to remove air humidity contribution at a resolution of 4cm^{-1} and 16 times scanning for each measurement to obtain an adequate signal to noise ratio.

Antibacterial activity against isolated bacterial strains

Optimized formulae were tested for their antibacterial potential on living isolated bacteria strains. The selected strains were gram-positive bacteria: *Staphylococcus Aureus* (*Staph A*) and gram-negative bacteria: *Escherichia Coli* (*E Coli*). The antibacterial activity was determined using the agar well diffusion method in *Mueller Hinton medium*.

The microorganisms were sub-cultured in *Tryptone Soya Broth* (TSB) for *Staph A* and *Luria Bertani broth* (LB) for *E Coli*. After 24 h of incubation period, the bacterial count was adjusted at 0.5 *McFarland* (corresponding to $1.5*10^8$ CFU/mL). Five drops of broth were seeded in the sterile glass petri dishes (15*90 mm) using sterile *Pasteur* pipettes. Nutrient agar was freshly prepared then poured on the microorganisms and mixed well [25].

Wells, of 13mm diameter each, were made in the plates using sterile cork borers. Exact volumes of the selected FA-AgNPs (F_{14}) and cef.Na-FA-AgNPs ($F_{14}B$) containing each 1µM $AgNO_3$ were added to the corresponding well. An accurate volume of cef.Na containing the same amount present in $F_{14}B$ was also used. Sterile saline served as the negative control in each plate.

The culture plates were incubated at 37°C for 24h in an incubator, (*SHEL LAB, model 1555, SHELDON, USA*). The plates were then removed and zones of inhibition measured using *Vernier Caliper* and results tabulated. Each experiment was carried out in triplicates. Means (±s.d) of the inhibition zones were used to calculate the antimicrobial activity of the corresponding sample.

Cell viability study

Cell culture

Fibroblast normal cell line HFB4 was maintained in *Dulbecco's Modified Eagle's Medium* (DMEM) supplemented with 100 µg/mL streptomycin, 100 units/mL penicillin and 10% heat-inactivated fetal bovine serum in a humidified, 5% (v/v) CO_2 atmosphere at 37 ºC.

MTT assay

Cells were seeded at a density of 2000 cells/ well in 96-well plates. After achieving confluency, cells were exposed to different treatments, each prepared at five different concentrations, for 72h. Cell cytotoxicity was assessed at the end of NPs exposure using MTT assay, based on tracking viable cells able to convert MTT into formazan crystals determined spectrophotometrically. Absorbances were measured at 570nm using microplate reader (*BioTek instruments, Vermont, USA*). Results were expressed as the relative percentage of absorbance compared to control [26]. Experiments were done in triplicates for each plain Ag-NPs prepared using TSC or FA (F_{14}), as well as cef.Na loaded FA-AgNPs ($F_{14}B$). Half-maximal inhibitory concentration (IC_{50}), the Ag-NPs concentration at which 50% growth inhibition is achieved, was calculated using *Graph Pad Prism software*, version 5.00 (*GraphPad Software, Inc. La Jolla, CA, USA*).

Pharmacodynamic activity of selected formulae on rats

A pharmacodynamic study was conducted to evaluate the antimicrobial and wound healing enhancing activity of the selected formulae on injured rats. Male albino rats, obtained from the animal house of the *Animal Experimental Unit*, were housed under standard experimental conditions. The experimental procedures conformed to the *Ethics Committee* no. 182, of *Faculty*

of Pharmacy, Ain Shams University on the use of animals which is in accordance with the U.K. Animals (Scientific Procedures) Act, 1986 and associated guidelines, EU Directive 2010/63/EU for animal experiments.

Rats were kept at controlled temperature of 25±0.5°C, with 12h light–dark cycles, and fed on normal pellet diet and water *ad* libitum. Prior to the experiment, the dorsal area of each mouse was carefully shaved and the exposed skin disinfected with iodine. Near the neck posterior surface, the injury was made as a circular full thickness excision wound with 15mm diameter and 2mm depth [27]. Sterile scissors and surgical blades were used. The wound was infected using 10µL of each *Staph A* and *E Coli* adjusted at 0.5 *macfarland* (10^8CFU/mL) on day zero [28]. The bacterial inoculum was placed at the center of the wound and spread using a pipette tip to cover the wound area. The treatment started 24h after injury.

Three non-wounded rats served as control in biochemical marker study, whereas wounded animals were divided into three groups (I, II, III), receiving the assigned treatment daily according to the following protocol:

- **Group I,** (n=12) negative control group: Untreated animals
- **Group II,** (n=9) positive control: Animals treated with marketed cef.Na solution (*Claforan*®) applied topically.
- **Group III,** (n=9): Animals treated with cef.Na-FA-AgNPs ($F_{14}B$).

Wound area contraction

The wound area was determined by measuring the diameter of the open wound surface using a *Vernier Caliper*; the wound healing percentage was calculated by the Walker formula. The percentage of wound healing was computed on days 0, 7, and 14. The wound closure percent was calculated as follows [29]:

$$\text{Wound closure } \% = \left(1 - \frac{\text{open wound area}}{\text{initial wound area}}\right) * 100 \qquad \text{Eq. (1)}$$

Macroscopic wound area evaluation

Prior to dose application, photographic images were taken using a digital camera to record wound area on days 0, 7, and 14 applying the same camera settings and under the same conditions each time [30].

Histopathologic examination

Three rats were sacrificed from each group on day 0, 7, and 14, the cross-sectional full-thickness specimens of skins were excised from healed wounds and surrounding tissues [31]. Samples were fixed in 10% formal saline for 24h, processed using a paraffin tissue-processing machine, then 5µm sections were stained with *hematoxylin and eosin* (H&E) stain [29]. Epithelialization, angiogenesis, inflammatory cell infiltration, fibroplasia and granulation tissue formation were assessed in different groups, comparatively.

Biochemical markers determination

Prior to dissection, the wound tissues were perfused with a phosphate buffered saline solution, pH 7.4 containing 0.16mg / mL heparin to remove any red blood cells and clots. The tissues were then homogenized in 5–10mL cold buffer (50mM potassium phosphate, pH 7.5) per gram tissue. The homogenizate was centrifuged at 4000 rpm for 15 m and the supernatant removed for assay. If not assayed on the same day, samples were frozen at -80°C [32].

Determination of malondialdehyde (MDA)

MDA is used as a marker for lipid peroxidation and was determined using a standard colorimetric method which depends on the reaction of Thiobarbituric Acid (TBA) with MDA in acidic medium at temperature 95°C for 30 min to form TBA reactive product. The absorbance of the resultant pink product can be measured at 534nm [33,32].

$$MDA\ (n\ mol\ e/m\ g\ tissue) = \frac{A_{sample}}{A_{standard}} * \frac{10}{mg\ of\ tissue\ used} \qquad \text{Eq. (2)}$$

Determination of superoxide dismutase (SOD)

The antioxidant activity was evaluated by determination of SOD. The assay relies on the ability of SOD enzyme to inhibit the phenazine methosulphate-mediated reduction of nitroblue tetrazolium dye [34]. The SOD activity was calculated using the following equation:

$$SOD\ (U/m\ g\ tissue) = \%\ inhibition * 3.75 * \frac{1}{mg\ tissue\ used} \qquad \text{Eq. (3)}$$

Statistical analysis

All Data are expressed as mean of three determinations ± standard deviation (s.d). The experimental data were analyzed statistically using Graph Pad Prism program by which either the *Paired Student's t-test* (comparison between means of two groups) or by analysis of variance (*ANOVA*, for more than 2 groups) were performed followed by *Bonferroni* multiple comparison test. Differences were considered significant at $P \leq 0.05$.

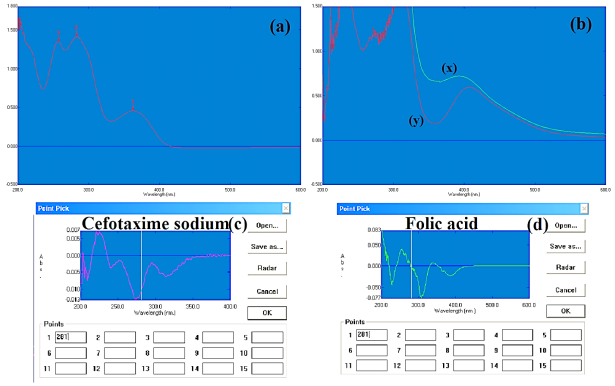

Figure 1: Ultraviolet spectra of **(a)**: FA showing λmax at 348, 281, and 256nm.
(b): dialyzed F_{14} measured versus DW (x) and FA (y) as blank
(c) and **(d)**: cef.Na and FA in PB using 1st derivative technique at 281 nm.

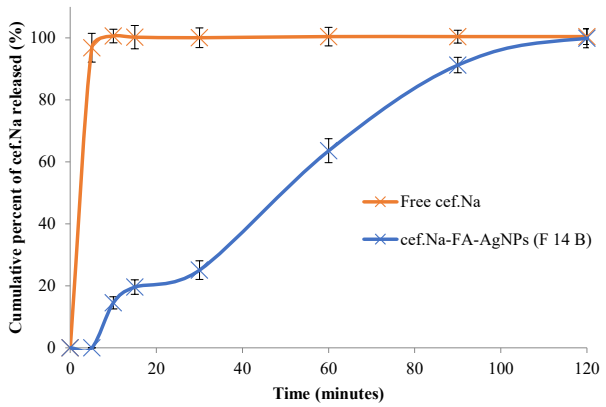

Figure 2: Ultraviolet spectra of **(a)**: FA showing λmax at 348, 281, and 256nm.
(b): dialyzed F_{14} measured versus DW (x) and FA (y) as blank
(c) and **(d)**: cef.Na and FA in PB using 1st derivative technique at 281 nm.

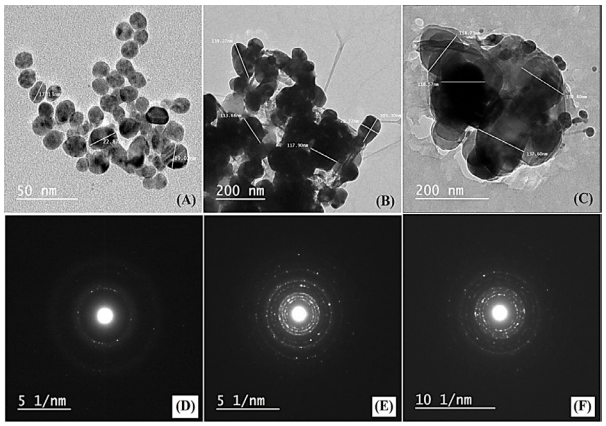

Figure 3: TEM imaging and selected area electron diffraction of citrate- AgNPs **(A & D)**, FA- AgNPs **(B & E)** and cef.Na-FA-AgNPs **(C & F)**.

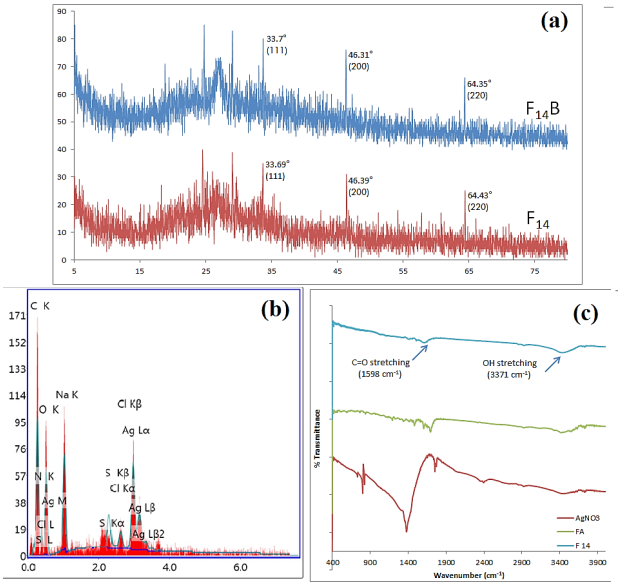

Figure 4: (a): XRPD of blank FA-AgNPs (F_{14}) and cef.Na-FA-AgNPs (F_{14}B). (b) electron dispersed X-ray (EDX) analysis of F_{14}B. (c) FT-IR of pure components: $AgNO_3$, FA, and the selected plain FA-AgNPs (F_{14}).
The compositions of F_{14} and F_{14}B are shown in Tables 1 and 2.

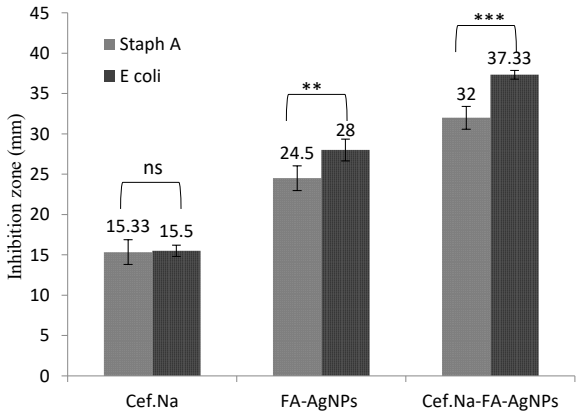

Figure 5: *In-vitro* antibacterial activity of optimized FA-AgNPs on *Staph A* and *E Coli* using the agar well diffusion method.
For composition, refer to Tables 1 and 2. The inhibition zone was measured using a caliper. Results are expressed as mean ±s.d (n=3). Statistical analysis was carried out to compare the antimicrobial activity of each formula against both microorganisms using *ANOVA* followed by *Bonferroni* multiple comparison test **: *P*<0.01, ***: *P*<0.001, ns: non-significant.

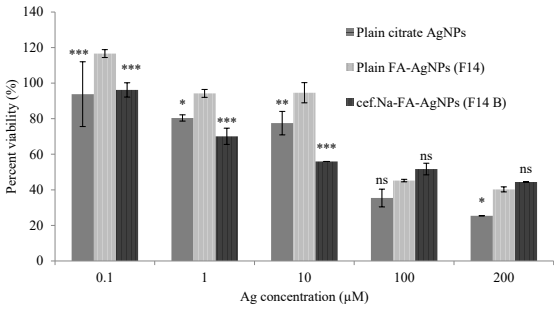

Figure 6: Cell viability of AgNPs on fibroblast normal cell line (*HFB4*).
Formulae codes and compositions are shown in Tables 1 and 2. Results are expressed as mean ± s.d (n=3). Statistical analysis was carried out using *ANOVA* followed by *Bonferroni* multiple comparison test comparing conventional citrate-AgNPs and cef. Na-FA-AgNPs to FA-AgNPs. *: *P*<0.05, **: *P*<0.01, ***: *P*<0.001, ns: non-significant.

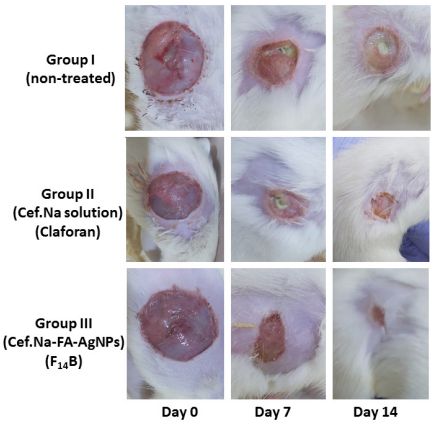

Figure 7: Photographic images of the wound surface.
Group I: negative control, group II: positive control (cef.Na solution *Claforan*®), group III: cef.Na-FA-AgNPs (F_{14}B).

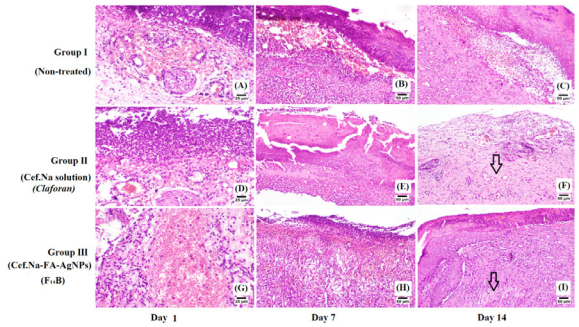

Figure 8: Histopathological photomicrographs of rat skin in groups I, II & III at days 1, 7 & 14 using H&E stain showing:
A), D) & G) Acute inflammatory reaction and neutrophils infiltration with excessive edema with fibrinous exudates, hemorrhages and serocellular crust.
B) Heavy inflammatory cells infiltration with necrotic crust and abundant hemorrhages covering the wound surface.
C) Thick necrotic crust with underneath edema and inflammatory cells infiltration.
E) Serocellular crust covering with heavy inflammatory cells infiltration.
F) Less inflamed collagen rich (black arrow) well-vascularized filling granulation tissue.
H) Partially organized fibrovascular tissue with moderate hemorrhages filling the wound gap.
I) Abundant collagen depositions in the wound gap with epidermal remodeling at the wound edge.

Table 1: Composition, PS, ζ and λ_{max} of FA-stabilized AgNPs.

Code	$AgNO_3$/FA* (M ratio)	FA/$NaHCO_3$	PS ±s.d (nm)	PDI ±s.d	λ_{max} ±s.d (nm)	ζ ±s.d (mV)
F_1	1:1	1:1	516.3±52.6	0.696±0.03	439.2±0.3	-30.7±1.6
F_2		1:2	573.0±53.8	0.684±0.03	443.0±0.2	-30.2±2.4
F_3		1:4	494.5±82.5	0.593±0.03	445.0±0.2	-29.7±2.7
F_4		1:8	584.3±26.9	0.746±0.02	445.7±0.5	-27.5±2.2
F_5	1:2.5	1:1	526.6±46.8	0.746±0.06	427.6±0.5	-34.7±2.0
F_6		1:2	246.3±27.4	0.643±0.05	434.8±0.5	-31.1±1.1
F_7		1:4	247.1±29.7	0.705±0.06	436.4±0.3	-29.8±1.1
F_8		1:8	540.2±48.3	0.752±0.06	438.8±0.5	-28.2±1.4
F_9	1:5	1:1	333.6±88.5	0.600±0.05	421.0±0.3	-44.5±1.5
F_{10}		1:2	268.2±71.3	0.579±0.03	425.6±0.5	-39.0±2.2
F_{11}		1:4	280.3±31.8	0.583±0.03	433.2±0.3	-32.5±3.6
F_{12}		1:8	358.4±55.2	0.577±0.04	433.9±0.2	-28.9±2.8
F_{13}	1:10	1:1	275.2±68.0	0.363±0.03	419.0±0.3	-45.6±1.1
F_{14}		1:2	119.8±33.9	0.398±0.01	420.5±0.4	-42.7±2.7
F_{15}		1:4	236.6±31. 9	0.329±0.04	426.6±0.6	-33.8±2.4
F_{16}		1:8	258.3±17.3	0.386±0.03	428.5±0.6	-29.1±1.2
F_{17}	1:20	1:1	469.1±52.4	0.463±0.02	411.5±0.3	-40.9±3.0
F_{18}		1:2	249.9±40.5	0.558±0.02	412.0±0.4	-35.5±3.3
F_{19}		1:4	260.8±22.3	0.442±0.02	412.2±0.3	-28.4±2.1
F_{20}		1:8	741.9±23.1	0.453±0.04	412.5±0.7	-25.1±4.0
F_{21}	1:30	1:1	408.2±23.8	0.835±0.07	409.5±0.3	-39.1±0.8
F_{22}		1:2	281.7±37.3	0.686±0.04	410.0±0.5	-33.1±3.7
F_{23}		1:4	257.8±64.7	0.722±0.07	410.2±0.3	-23.4±2.0
F_{24}		1:8	720.0±32.3	0.566±0.04	410.5±0.5	-18.2±0.4

* FA/ $NaHCO_3$ weight ratio. $AgNO_3$ was kept at 1mM in all formulae.
Statistical analysis was carried out using *ANOVA* followed by *Bonferroni* multiple comparison test

Table 2: Effect of loading cef.Na on the characteristics of FA-AgNPs

Code	cef.Na/$AgNO_3$	PS ±s.d (nm)	PDI ±s.d	λ_{max}± s.d (nm)	ζ ±s.d (mV)
F_{14}	-	119.8±9.4	0.398±0.02	420.5±0.4	-42.7±2.7
$F_{14}A$	1:10	222.1±8.7***	0.539±0.03**	426.6±0.4*	-31.9 ±1.9*
$F_{14}B$	1:5	453.6±7.0***	0.519±0.02***	427.0±0.4**	-28.9 ±0.8*

Results are expressed as mean ± s.d (n=3). Cef.Na:$AgNO_3$ is molar ratio. F_{14} prepared prepared with $AgNO_3$/FA=1:10 & FA/$NaHCO_3$=1:2. Statistical analysis was carried out using *Paired Student's t-test*,*: $P<0.05$, **: $P<0.01$, ***: $P<0.001$. F_{14} used in preparation was dialyzed.

Table 3: Wound area and biochemical markers levels at the wound site of the wounded rats.

Group	Treatment	Parameter	Measured parameter at			Change in parameter level (%)
			1 day	7 days	14 days	
I	No treatment	area± s.d	1.767±0	1.100 ±0.22	0.680 ±0.10	61.51
		MDA [a]± s.d	5.47±0.74	3.22±0.42	2.63±0.43	-51.91
		SOD [b]± s.d	1.20±0.39	2.14±0.42	2.14±0.46	78.33
II	Cef.Na solution *(Claforan®)*	area± s.d	1.767±0	0.790 ±0.13**	0.480 ±0.18ns	72.83
		MDA± s.d	5.47±0.74	3.14±0.35 ns	2.38±0.41 ns	-56.48
		SOD± s.d	1.20±0.39	1.83±0.30 ns	2.04±0.33 ns	70
III	Cef.Na-FA-AgNPs ($F_{14}B$)	area± s.d	1.767±0	0.736 ±0.17**	0.244 ±0.13***	86.19
		MDA± s.d	5.47±0.74	1.93±0.17 **	1.57±0.37 *	-71.30
		SOD± s.d	1.20±0.39	3.13±0.87*	3.88±0.95***	223.33

F_{14}: FA-AgNPs. F_{14}B: cef.Na-FA-AgNPs. For composition, refer to Tables 1 and 2.
Group I: negative control, group II: positive control. Statistical analysis was carried out using *ANOVA* to compare each of the treated groups with the non-treated group I followed by *Bonferroni* multiple comparison test, *: P<0.05, **: P<0.01, ***: P<0.001, ns: non-significant. Results expressed as mean ±s.d (n=3). a: malondialdehyde b: superoxide dismutase Normal MDA value: 0.85 ±0.32. Normal SOD value: 5.02±0.41. Parameters are measured in: area= mm^2, MDA = n mole/mg tissue, SOD= Unit/mg tissue.
% change in marker level was calculated as percent of the initial as follow $\frac{Final\ value\ at\ day\ 14 - Initial\ value\ at\ day\ 1}{Initial\ value\ at\ day\ 1} * 100$

Results and discussion

AgNPs preparation using FA

As previously outlined, FA has several advantages in tissue repair when topically applied. To the best of our knowledge FA was used, for the first time in this work, as reducing agent during the preparation of AgNPs. The appearance of the characteristic yellow color of Ag-NPs evidenced their successful formation. Due to its substantial role in solubilizing FA, $NaHCO_3$ concentration was varied (Table 1). At all $AgNO_3$/FA ratios, except the 1:1 ratio, FA/$NaHCO_3$ ratios of 1:2 and 1:4 yielded FA-AgNPs with significantly smaller PS varying from 119.8±33.9 to 281.7±37.3nm. Lager sized AgNPs were formed compared to their conventional analogues prepared using small molecules (TSC) 33.3±0.5 nm (*results not shown in table*), conveying with the literature reporting such small PS using TSC or sodium borohydride reducing molecules [35,36].

PDI values ranged from 0.329 to 0.835, with the smallest values (from 0.329 to 0.398) seen at $AgNO_3$/FA ratio 1:10 (P<0.001). In accordance to literature, λ_{max} of all formulae ranged between 409.5 and 445.7nm, proving the formation of colloidal AgNPs, [37,38]. A decline of ζ with increasing $NaHCO_3$ amounts was evident, probably due to sodium ion adsorption. Relatively higher ζ were noted at $AgNO_3$/FA ratio 1:10 compared to the other ratios. In addition, a higher ζ was recorded in comparison to the Ag-NPs prepared with trisodium citrate (-5.2±0.7 mV) (*results not shown in table*) due to FA presence. Based on the previous data, formula F_{14}, prepared at ratios of $AgNO_3$/FA of 1:10 and FA/$NaHCO_3$ of 1:2, scoring respective PS, PDI, ζ of 119.8±33.9nm, 0.398±0.01, -42.7±2.7mV, was selected for subsequent drug loading studies. This formula was evaluated for stability for 2 weeks storage at 4°C where a significant PS and PDI increase were seen P<0.001 (209.8±13.3nm) and P<0.05 (0.431±0.02) respectively, with no significant changes in λ_{max} and ζ (P>0.05) (*data not shown in table*). Accordingly, F_{14} was dialyzed for 24 h to remove excess FA. The dialyzed formula showed non-significant differences in PS (122±15.87nm) after two months confirming a greater stability than non-dialyzed F_{14} (*data not tabulated*).

The presence of FA within AgNPs was proved by the larger size and high ξ, even after dialysis, than those prepared with TSC. The presence of FA entrapped within plain dialyzed AgNPs was also proved spectrophotometrically by the presence of λ_{max} 364 Figure 1(b). Though this FA peak was shifted from the original λ of 348nm for FA alone due to AgNPs formation Figure 1(a), it confirmed the colocation of FA and AgNPs in the prepared dialyzed AgNPs by the use of FA.

Cef.Na loaded FA-AgNPs

Cef.Na was loaded by direct incubation with FA-AgNPs for 24h to allow for drug adsorption and conjugation [39,40]. In addition, possible hydrogen bond between –NH group of the drug and -COOH group of FA might had taken part in excessive drug loading [41,42]. To avoid interference between the drug and FA previously proved to be intercalated between AgNPs crystals spectrophotometric drug determination using the 1st derivative was adopted [43]. Cef.Na absorbances were determined at 281nm, Figure 1(c), and then the calibration curve was constructed in PB (*data not shown).*

Based on previous experiences, two molar ratios of cef.Na/$AgNO_3$, 1:10 and 1:5, were tried [44], Table 2. The PS of drug loaded F_{14}A and F_{14}B were significantly higher compared to the plain formula, delineating successful drug deposition [45]. Compared to plain (F_{14}), PDI showed significant rise at P<0.01 and P<0.001 in F_{14}A and F_{14}B, respectively. Cef.Na amino groups imparted a positive net charge to the particles leading to the significant decrease in ζ absolute values (F_{14}A and F_{14}B compared to F_{14}) [46]. Higher drug loading was concluded in F_{14}B due to comparatively larger PS and lower ζ. The exact values for drug loading could not be determined as long dialysis time and high dilutions needed, may lead to the drug desorption. Previous studies reported a direct relation between NPs size and penetration depth through the skin layers, favoring larger PS for topical drug use [47]. Accordingly F_{14}B was selected for further studies. In addition the formula proved a good stability due to non-significant changes over two weeks storage at 4°C for PS, PDI and λ_{max}. Finally, a significantly slower release profile was noticed for loaded drug confirming its successful loading, Figure 2 [48].

Transmission electron microscope (TEM) imaging

Figure 3(A) shows the classic dark spherical uniform non-aggregated particles with size ranging between10 and 30nm of the well-known AgNPs prepared with TSC at pH 6,7[49] [50]. It was reported that the NPs shape depended mainly on the pH [49]. Here in the solution pH was 4.3 due to FA (*pH meter, Jenway, type 3310, UK*), producing angle polygonal shaped particulates, Figure 3(B) [45]. Cef.Na-FA-AgNPs (F_{14}B) shows larger particles with aggregation probably due to cef.Na loading leading to crosslinking between neighboring FA-AgNPs Figure 3(C).

The Selected Area Electron Diffraction (SAED) is a recent crystallographic experimental technique inside TEM used for the determination of crystal phases. SAED of TSC AgNPs shows three diffraction rings of face centered cubic AgNPs namely: (111), (200) and (220) Bragg diffraction Figure 3(D) [51], compared to a quasi-ring-like diffraction pattern in Figure 4(E&F), demonstrating that a polycrystalline structure was obtained with FA [52]. The novel green synthesized FA-AgNPs revealed the characteristic rings of face centered NPs beside more numerous other rings. This increased crystallinity has been always associated with greater shelf life stability.

X ray powder diffraction (XRPD)

Characteristic sharp peaks of $AgNO_3$, FA and cef.Na reflect their crystalline nature (*data not shown*). In spite of their freeze drying, Figure 4(a) reveals the semi crystalline nature of FA-AgNPs and cef.Na-FA-AgNPs. The characteristic Ag peaks were recorded at ~ 23°, 29°, 33°, 46° and 64°. Peaks at 33°, 46° and 64° correspond to (111), (200) and (220) Bragg reflections of

crystalline AgNPs, respectively [53]. This semi crystalline structure discloses the experimental conditions effects on nucleation and nuclei crystal growth.

Energy dispersive X-ray analysis

It is generally used to reveal the purity and complete chemical composition of the sample [24]. Figure 4 (b) shows the percentage relative composition of elements in Cef.Na-FA-AgNPs ($F_{14}B$): carbon (33.25%), oxygen (28%), nitrogen (14.27%), silver (11.83%), sodium (10.74%) and sulphur (1.91%). Signals from the silver atoms are seen at 3keV [54]. In addition a small peak at 8keV corresponding to traces of copper from the copper grid used for measurement was also present [55]. The sulphur peak at 2.2KeV is most probably due to the two sulphur atoms in cef. Na structure [56]. Furthermore, the high carbon and oxygen signals denoted the presence of FA, reducing anabolic agent, as previously reported while using plant extracts for the preparation of AgNPs [57,58], besides the carbon coat of the grid used [59].

FT-IR

FT-IR spectra of $AgNO_3$, FA, and cef.Na revealed their characteristic peaks, Figure 4(c). The disappearance of symmetric and asymmetric NO stretching peaks (seen with $AgNO_3$ spectrum) is indicative of complete reduction of silver ions to AgNPs in both, FA-AgNPs (F_{14}) and cef.Na-FA-AgNPs ($F_{14}B$); moreover, the presence of absorption peaks at 3381, 2873, 1578, 1348 cm^{-1} confirms the formation of Ag-NPs [60]. The shift of the peaks positions compared to their components points towards the interaction between the reduced Ag and these groups [61].

Furthermore, the spectrum of dialyzed F_{14} plain FA-AgNPs revealed FA characteristic peaks of C=O stretching at 1598 cm^{-1} and OH stretching at 3371 cm^{-1}. The presence of such groups in dialyzed formula postulates the successful incorporation of sufficient FA molecules with their intact COOH groups.

Antibacterial activity

Figure5 proved that cef.Na is active against both *Staph A* and *E Coli*. Researchers suggested a slightly stronger activity against gram-negative rather than gram-positive organisms [62], others reported the contrary [63]. Moreover, FA-AgNPs shows larger inhibition zones than cef.Na solution with both types of microorganisms. The significant increase in inhibition zone (P<0.001) noted with cef.Na-FA-AgNPs ($F_{14}B$) was due to the combined antimicrobial activity of AgNPs and cef.Na. In addition, cef.Na-FA-AgNPs revealed larger inhibition zones with *E coli* compared to *staph A*, demonstrating a higher activity against gram-negative than gram-positive organisms [64]. The thickness of the peptidoglycan cell wall in the two bacteria types are: 30nm in gram-positive and 3-4nm in gram-negative bacteria. Hence, cell wall penetration of AgNPs in gram-negative would be easier [7].

Cell viability study

The cell viability study was performed to evaluate the effect of FA incorporation in Ag-NPs in terms of safety. Generally, significantly higher cell viability percentages were noticed with plain FA-AgNPs than the corresponding TSC-AgNPs, proving folate anabolic activity, Figure 6. Furthermore, the addition of cef.Na produced statistically significant decrease in cell viability at concentrations below 100µM. Non-significant differences between percentage cell viability were noticed at higher silver concentration due to increased silver toxicity. However, the smaller sized TSC-AgNPs might be the cause of its increased toxicity at the highest Ag concentrations (200µM).

Wound healing activity of the selected formulae

Wound area contraction and photography

Infected excision wounds in animals were weekly evaluated for wound area and percent wound closure for 2 weeks. Table 3 shows a 61.8% wound area closure after two weeks in group II treated with drug solution (*Claforan*®) which was statistically significant smaller area compared to group I only on day 7 (P<0.01). Actually, the antibiotic does not affect or take part in the wound healing process itself it only prevents or treat the infection that could delay wound healing. However drug loaded FA-AgNPs, group III achieved a wound area contraction exceeding 85%. A clean non-inflamed wound was observed since day 7, evidencing the synergistic activity of the platform combination of AgNPs, cef.Na previously proved to have a synergistic antibacterial activity, added to the anabolic and wound enhancing activity of FA. Figure 7 shows the photographic images of the groups along the study period where the smallest open wound surface was seen with group III with the least exudate and the healthiest non-scar healed wound. Infected exuding open wound was noted in group I along the study period.

Histopathologic examination

The histopathologic sections of the wounded animals confirmed the previous findings. Acute inflammatory reaction and massive neutrophil infiltration with edema, hemorrhages and fibrinous infiltration were obvious on day 0 (Figure 8(A,D&G). Thick serocellular crust was also observed in all examined sections associated with numerous transmigrated neutrophils [29]. Figure 8(B) shows delayed signs of wound healing, including absence of re-epithelization with necrotic tissue debris on day 7 in the untreated group I. The wound gap was also filled with unhealthy severely inflamed granulation tissue. Newly formed blood capillaries were less frequently detected. On day 14, Figure 8(C), shows the beginning of a poor healing.

Group II (cef.Na solution (*Claforan*®) treated group) Figure 8(E) depicts mild improvement in healing criteria, where few collagen deposition was noticed in some sections associated with numerous mononuclear inflammatory cells infiltrations on day 7. The base of the wound displayed excessive hemorrhages in some circumstances, with abundant serocellular crust at the surface, accompanied by intense infiltrated neutrophils. On day 14, Figure 8(F) demonstrates remarkable improvement in wound healing compared to group I (untreated group) could be noted. The wound cavity showed more collagen deposition with variable number of inflammatory cells infiltration, indicating early stages of wound healing [29].

The wound area in group III (cef.Na-FA-AgNPs treated group) Figure 8(H) on day 7 was filled with granulation tissue along with more collagen content. In spite of some hemorrhagic areas, the inflammation was moderate. Finally, on day 14, marked wound healing was evidenced among several examined sections, Figure 8(I). The wound gap was filled with abundant collagenous matrix in addition to numerous reactive fibroblasts and less inflammatory cells infiltration. The wound surface showed enhanced covering with epidermal remodeling in several examined sections. Collagen synthesis is reported to be stimulated by FA included in the NPs helping in better wound healing [4].

Biochemical markers

Increasing in MDA (oxidation product) is noticed always at

high oxidative stress. Following wound initiations, the measured MDA levels were significantly high up to 5.47±0.74 n mole/mg tissue, compared to 0.85 ±0.32 n mole/mg tissue (normal values), Table 3. In all the animal groups, significant drops in MDA level occur on day 7 compared to day 0 at $P<0.001$ with non-significant changes at day 14 ($P>0.05$).

SOD is an endogenous antioxidant molecule, having the capability to scavenge free radicals with normal level of 5.02±0.41 Unit/mg. It scored low levels in wounded animals (1.20±0.39 Unit/mg) and increased as healing proceeds. The highest significant increase ($P<0.001$) was noticed with cef.Na-FA-AgNPs delineating an anti-oxidant activity for the used cef.Na-FA-AgNPs mainly due to the presence of FA [65].

Conclusion

An environmentally friendly green method using the anabolic FA was adopted to reduce $AgNO_3$. The chosen formula ($F_{14}B$) scoring a size of 453.6±7nm and ζ of -28.85 ±0.777mV was loaded with cef.Na. FA was proved to be intercalated in the prepared colloidal silver NPs. An advantage which lead to better wound closure due to the high collagen stimulating activity of FA. Furthermore, FA played an important role in oxidative stress reduction proved by MDA decrease and SOD increase with an enhanced collagens synthesis as manifested by macroscopic and histopathologic examination. The results endorse the superiority of the suggested platform for better critical wound management.

Future perspective

Cef.Na-FA-AgNPs formula prepared with FA represents promising and efficient platform for wound treatment. An efficiency which can be further improved by the use of bio inspired sustained drug delivery system to ensure a prolonged contact with wound surface targeting with less painful application for better patient compliance [66].

References

1. X Deng, M Gould, M A Ali. A review of current advancements for wound healing: Biomaterial applications and medical devices, J. Biomed. Mater. Res. Part B Appl. Biomater. 2022; 110(11): 2542-2573.
2. D Fernández-Villa M, Jiménez Gómez-Lavín C, Abradelo J, San Román, L Rojo. Tissue engineering therapies based on folic acid and other vitamin B derivatives. Functional mechanisms and current applications in regenerative medicine, Int. J. Mol. Sci. 2018; 19(12): 4068.
3. M ZHAO, et al. Folic Acid Promotes Wound Healing in Diabetic Mice by Suppression of Oxidative Stress, J. Nutr. Sci. Vitaminol. (Tokyo). 2018; 64(1): 26-33. doi: 10.3177/jnsv.64.26.
4. M Bagheri, B Moein Jahromi, A Zamani. Folic acid may be a potential addition to diabetic foot ulcer treatment - a hypothesis, Int. Wound J. 2011; 8: 658-660. doi: 10.1111/j.1742-481X.2011.00830.x.
5. K Kida, M Tomotake, H Sasako, Y Matsuda, N Sasaki, et al. Small amounts of ethanol attenuate folic acid stability in acidic beverages during storage., Food Sci. Nutr. 2018; 6(1): 214-219. doi: 10.1002/fsn3.549.
6. T Bruna, F Maldonado-Bravo, P Jara, N Caro. Silver nanoparticles and their antibacterial applications, Int. J. Mol. Sci. 2021; 22(13): 7202.
7. S A Polash, M Hossain, T Saha, S R Sarker. Biogenic Silver Nanoparticles: A Potent Therapeutic Agent, in Emerging Trends in Nanomedicine, Springer. 2021; 81-127.
8. E S Al-Sheddi, et al. Anticancer Potential of Green Synthesized Silver Nanoparticles Using Extract of Nepeta deflersiana against Human Cervical Cancer Cells (HeLA), Bioinorg. Chem. Appl. 2018; 9390784. doi: 10.1155/2018/9390784.
9. O Akintola, et al. Antioxidant properties of silver nanoparticles biosynthesized from methanolic leaf extract of Blighia sapida, in IOP Conference Series: Materials Science and Engineering. 2020; 805(1): 12004.
10. D Garibo, et al. Green synthesis of silver nanoparticles using Lysiloma acapulcensis exhibit high-antimicrobial activity, Sci. Rep. 2020; 10(1): 12805. doi: 10.1038/s41598-020-69606-7.
11. N S Alharbi, N S Alsubhi. Green synthesis and anticancer activity of silver nanoparticles prepared using fruit extract of Azadirachta indica, J. Radiat. Res. Appl. Sci. 2022; 15(3): 335-345. doi: https://doi.org/10.1016/j.jrras.2022.08.009.
12. F Lalsangpuii, et al. Green Synthesis of Silver Nanoparticles Using Spilanthes acmella Leaf Extract and its Antioxidant-Mediated Ameliorative Activity against Doxorubicin-Induced Toxicity in Dalton's Lymphoma Ascites (DLA)-Bearing Mice, ACS Omega. 2022; 7(48): 44346-44359. doi: 10.1021/acsomega.2c05970.
13. L M Stabryla, et al. Role of bacterial motility in differential resistance mechanisms of silver nanoparticles and silver ions, Nat. Nanotechnol. 2021; 16(9): 996-1003. doi: 10.1038/s41565-021-00929-w.
14. M Afridi, et al. Combining antibiotics with silver nanoparticles: A potential treatment strategy against antimicrobial resistance, Main Gr. Chem. 2021; 21: 1-22. doi: 10.3233/MGC-210131.
15. S H Haji, F A Ali, S T H Aka. Synergistic antibacterial activity of silver nanoparticles biosynthesized by carbapenem-resistant Gram-negative bacilli, Sci. Rep. 2022; 12(1): 15254. doi: 10.1038/s41598-022-19698-0.
16. S Zakaria, S A Afifi, K A Elkhodairy. Newly developed topical cefotaxime sodium hydrogels: antibacterial activity and in vivo evaluation, Biomed Res. Int. 2016.
17. E Ephrem, H Greige-Gerges, H Fessi, C Charcosset. Optimisation of rosemary oil encapsulation in polycaprolactone and scale-up of the process, J. Microencapsul. 2014; 31(8): 746-753.
18. L Cole, D Fernandes, M T Hussain, M Kaszuba, J Stenson, et al. Characterization of recombinant Adeno-Associated Viruses (rAAVs) for gene therapy using orthogonal techniques, Pharmaceutics. 2021; 13(4): 586.
19. M S Mehata. Surface plasmon resonance allied applications of silver nanoflowers synthesized from Breynia vitis-idaea leaf extract. Dalt. Trans. (Cambridge, Engl. 2003). 2022.
20. W W Mustafa, J Fletcher, M Khoder, R G Alany. Solid Dispersions of Gefitinib Prepared by Spray Drying with Improved Mucoadhesive and Drug Dissolution Properties., AAPS PharmSciTech. 2022; 23(1): 48. doi: 10.1208/s12249-021-02187-4.
21. Y Zubairu, L M Negi, Z Iqbal, S Talegaonkar. Design and development of novel bioadhesive niosomal formulation for the transcorneal delivery of anti-infective agent: In-vitro and ex-vivo investigations, Asian J. Pharm. Sci. 2015; 10(4): 322-330. doi: https://doi.org/10.1016/j.ajps.2015.02.001.
22. N Mehrban, J Bowen. 5 - Monitoring biomineralization of biomaterials in vivo, R J B TM, E of B. and their P I V Narayan, Ed. Wood head Publishing. 2017; 81-110.

23. X Rong, F Qiu, C Zhang, L Fu, Y Wang, et al. Preparation, characterization and photocatalytic application of TiO2-graphene photocatalyst under visible light irradiation, Ceram. Int. 2015; 41(2): 2502-2511.

24. G Femi-Adepoju, A O Dada, K O Otun, A O Adepoju, O P Fatoba. Green synthesis of silver nanoparticles using terrestrial fern (Gleichenia Pectinata (Willd.) C. Presl.): characterization and antimicrobial studies, Heliyon. 2019; 5(4): e01543.

25. Y K Mohanta, S K Panda, R Jayabalan, N Sharma, A K Bastia, et al. Antimicrobial, Antioxidant and Cytotoxic Activity of Silver Nanoparticles Synthesized by Leaf Extract of Erythrina suberosa (Roxb.). Front. Mol. Biosci. 2017; 4(14). doi: 10.3389/fmolb.2017.00014.

26. J Van Meerloo, G Kaspers, J Cloos. Cell sensitivity assays: The MTT assay, Methods Mol. Biol. 2011; 731: 237-245. doi: 10.1007/978-1-61779-080-5_20.

27. Y Ramadan, M K El-Ashry, I A Bahei-Eldin, A S E D Soliman, N E El-Nefiawy, et al. The role of silver nanoparticles on accelerating healing of skin wounds in rats: histologiocal and immunohistochemical study., Ain Shams Med. J. 2021; 72(3): 533-553.

28. M Å Andersson, L B Madsen, A Schmidtchen, M Puthia. Development of an Experimental Ex Vivo Wound Model to Evaluate Antimicrobial Efficacy of Topical Formulations, International Journal of Molecular Sciences. 2021; 22(9). doi: 10.3390/ijms22095045.

29. M M Abdellatif, Y E Elakkad, A A Elwakeel, R M Allam, M R Mousa. Formulation and characterization of propolis and tea tree oil nanoemulsion loaded with clindamycin hydrochloride for wound healing: In-vitro and in-vivo wound healing assessment, Saudi Pharm. J. 2021; 29(11): 1238-1249.

30. P Basu, N Uttamchand, R Arunachalam, S Devi, M Inderchand. Characterization and Evaluation of Carboxymethyl Cellulose-Based Films for Healing of Full-Thickness Wounds in Normal and Diabetic Rats, ACS Omega. 2018; 3: 12622-12632. doi: 10.1021/acsomega.8b02015.

31. F Hamam, A Nasr. Curcumin-loaded mesoporous silica particles as wound-healing agent: An in vivo study, Saudi J. Med. Med. Sci. 2020; 8(1): 17.

32. N A M Ghonimi, K A Elsharkawi, D S M Khyal, A A Abdelghani. Serum malondialdehyde as a lipid peroxidation marker in multiple sclerosis patients and its relation to disease characteristics, Mult. Scler. Relat. Disord. 2021; 51: 102941. doi: https://doi.org/10.1016/j.msard.2021.102941.

33. J Aguilar Diaz De Leon, C R Borges. Evaluation of Oxidative Stress in Biological Samples Using the Thiobarbituric Acid Reactive Substances Assay. J. Vis. Exp. 2020; 159. doi: 10.3791/61122.

34. Hassan, et al. Oxidative Stress of Some Triazolopyrimidine Derivatives and their Nucleoside Analogues on Mcf-7 and A549 Cell Lines, Egypt. J. Chem. 2020; 63(1): 247-253.

35. P S Yerragopu, S Hiregoudar, U Nidoni, K T Ramappa, A G Sreenivas, et al. Chemical synthesis of silver nanoparticles using tri-sodium citrate, stability study and their characterization, Int. Res. J. Pure Appl. Chem. 2020; 21(3): 37-50.

36. U T Khatoon, A Velidandi, G V S Nageswara Rao. Sodium borohydride mediated synthesis of nano-sized silver particles: Their characterization, anti-microbial and cytotoxicity studies, Mater. Chem. Phys. 2023; 294: 126997. doi: https://doi.org/10.1016/j.matchemphys.2022.126997.

37. E Rodríguez, et al. Synthesis of silver nanoparticles using reducing agents obtained from natural sources (Rumex hymenosepalus extracts), Nanoscale Res. Lett. 2013; 8: 318. doi: 10.1186/1556-276X-8-318.

38. Patra, K Baek. Antibacterial Activity and Synergistic Antibacterial Potential of Biosynthesized Silver Nanoparticles against Foodborne Pathogenic Bacteria along with its Anticandidal and Antioxidant Effects, Front. Microbiol. 2017. doi: 10.3389/fmicb.2017.00167.

39. Kaur S Preet, V Kumar, R Kumar, R Kumar. Synergetic effect of vancomycin loaded silver nanoparticles for enhanced antibacterial activity, Colloids Surfaces B Biointerfaces. 2019; 176: 62-69. doi: https://doi.org/10.1016/j.colsurfb.2018.12.043.

40. Yaqub S Ali, S A Ditta, F Tanvir, S Ali, M Naz. Enhanced bactericidal activity of azithromycin-coated silver nanoprisms in comparison to their spherical-shaped counterparts, Micro Nano Lett. 2020; 15(12): 834-839. doi: https://doi.org/10.1049/mnl.2019.0704.

41. Onoda, et al. Stabilization of Carboxylate Anion with a NH O Hydrogen Bond: Facilitation of the Deprotonation of Carboxylic Acid by the Neighboring Amide NH Groups, Bull. Chem. Soc. Japan - bull chem soc jpn. 2004; 77: 321-329. doi: 10.1246/bcsj.77.321.

42. R P Sekar, E Kulandaivel, D Damayanthi, J Saranya. Formulation and Evaluation of Azathioprine Loaded Silver Nanoparticles for The Treatment of Rheumatoid Arthritis, Asian J. Biomed. Pharm. Sci. 2013; 3: 28-32.

43. O S Tabbouche, I Soukkariyyeh. First-order derivative ultraviolet spectrophotometry of imipenem-cilastatin formulations, J. Taibah Univ. Med. Sci. 2014; 9(3): 178-181. doi: https://doi.org/10.1016/j.jtumed.2014.01.006.

44. S Selselehjonban, et al. Physicochemical and pharmacological evaluation of carvedilol-eudragit(®) RS100 electrosprayed nanostructures. Iran. J. Basic Med. Sci. 2019; 22(5): 547-556. doi: 10.22038/ijbms.2019.34246.8139.

45. Varan, E Bilensoy. Cationic PEGylated polycaprolactone nanoparticles carrying post-operation docetaxel for glioma treatment, Beilstein J. Nanotechnol. 2017; 8: 1446-1456. doi: 10.3762/bjnano.8.144.

46. F Ofridam, N Lebaz, E Gagniere, D Mangin, A Elaissari. Effect of secondary polymer on self-precipitation of pH-sensitive polymethylmethacrylate derivatives Eudragit E100 and Eudragit L100, Polym. Adv. Technol. 2020; 31(6): 1270-1279.

47. Z Mardhiah Adib, S Ghanbarzadeh, M Kouhsoltani, A Yari Khosroshahi, H Hamishehkar. The Effect of Particle Size on the Deposition of Solid Lipid Nanoparticles in Different Skin Layers: A Histological Study. Adv. Pharm. Bull. 2016; 6(1): 31-36. doi: 10.15171/apb.2016.006.

48. M Rozalen, M Sánchez-Polo, M Fernández-Perales, T J Widmann, J Rivera-Utrilla. Synthesis of controlled-size silver nanoparticles for the administration of methotrexate drug and its activity in colon and lung cancer cells, RSC Adv. 2020; 10(18): 10646-10660.

49. Loiseau V, Asila G, Boitel-Aullen M, Lam M Salmain, S Boujday. Silver-based plasmonic nanoparticles for and their use in biosensing, Biosensors. 2019; 9(2): 78.

50. W Handayani, A S Ningrum, C Imawan. The Role of pH in Synthesis Silver Nanoparticles Using Pometia pinnata (Matoa) Leaves Extract as Bioreductor, in Journal of Physics: Conference Series. 2020; 1428(1): 12021.

51. E Escárcega-González, et al. In vivo antimicrobial activity of silver nanoparticles produced via a green chemistry synthesis using Acacia rigidula as a reducing and capping agent, Int. J. Nanomedicine. 2018; 13: 2349.

52. El-Adawya A, Husseina E R, Sheha S, Abdel-Samadb A, A Hassanc, et al. Synthesis and Thermoluminescence of Novel Ag-

3PO4: Ba2+ Nanophosphor as Gamma Radiations Detector. 2021.

53. N Nagar, V Devra. A kinetic study on the degradation and biodegradability of silver nanoparticles catalyzed Methyl Orange and textile effluents, Heliyon. 2019; 5(3): e01356. doi: https://doi.org/10.1016/j.heliyon.2019.e01356.

54. M S Khalil, et al. Fabrication of silver nanoparticles from ziziphus nummularia fruit extract: effect on hair growth rate and activity against selected bacterial and fungal strains, J. Nanomater. 2022.

55. W A Lotfy, B M Alkersh, S A Sabry, H A Ghozlan. Biosynthesis of silver nanoparticles by Aspergillus terreus: Characterization, optimization, and biological activities, Front. Bioeng. Biotechnol. 2021; 265.

56. M B Abd Elhaleem, A A Farghali, A A G El-Shahawy, F I A El-Ela, Z E Eldine, et al. Chemisorption and sustained release of cefotaxime between a layered double hydroxide and polyvinyl alcohol nanofibers for enhanced efficacy against second degree burn wound infection, RSC Adv. 2020; 10(22): 13196-13214.

57. K Okaiyeto, H Hoppe, A I Okoh. Plant-based synthesis of silver nanoparticles using aqueous leaf extract of Salvia officinalis: Characterization and its antiplasmodial activity, J. Clust. Sci. 2021; 32: 101-109.

58. K Takcı, M S Ozdenefe, S Genc. Green synthesis of silver nanoparticles with an antibacterial activity using Salvia officinalis aqueous extract, J. Cryst. Growth. 2023; 614: 127239.

59. M Alam. Analyses of biosynthesized silver nanoparticles produced from strawberry fruit pomace extracts in terms of biocompatibility, cytotoxicity, antioxidant ability, photodegradation, and in-silico studies, J. King Saud Univ. - Sci. 2022; 34(8): 102327. doi: https://doi.org/10.1016/j.jksus.2022.102327.

60. K Loganathan, G Kumar, V K Arivarasan, A Rahuman, B Rao. Streptomyces sp. LK3 mediated synthesis of silver nanoparticles and its biomedical application, Bioprocess Biosyst. Eng. 2013; 37. doi: 10.1007/s00449-013-0994-3.

61. W Wahab, A Karim, N La Nafie, I wayan Sutapa. Synthesis of Silver Nanoparticles using Muntingia calabura L. Extract as Bioreductor and Applied as Glucose Nanosensor, Orient. J. Chem. 2018; 34(6).

62. O B Payne, J E Ericson. Chapter 2 - Empiric Antimicrobials for Neonatal Sepsis, W E Benitz, P B B TI D, P Smith, Eds. Philadelphia: Elsevier. 2019; 15-25.

63. M F Al-Hakkani, et al. Cefotaxime removal enhancement via bionanophotocatalyst α-Fe2O3 using photocatalytic degradation technique and its echo-biomedical applications, Sci. Rep. 2022; 12(1): 1-20.

64. L C Yun'an, Qing et al. Potential antibacterial mechanism of silver nanoparticles and the optimization of orthopedic implants by advanced modification technologies, Int. J. Nanomedicine. 2018; 13: 3311.

65. G Bjelakovic, et al. Is folic acid supplementation to food benefit or risk for human health?: Pteridines. 2013; 24(3-4): 165-181. doi: doi:10.1515/pterid-2013-0024.

66. R Abdel-Gawad, R Osman, G A S Awad, N Mortada. Wound healing potential of silver nanoparticles embedded in optimized bioinspired hybridized chitosan soft and dry hydrogel, Carbohydr. Polym. 2024; 324: 121526. doi: https://doi.org/10.1016/j.carbpol.2023.121526.